HERIOT WATT UNIVERSITY

Heriot-Watt University

Heriot-Watt University
Research Gateway

Dichroism for orbital angular momentum using parametric amplification

Lowney, J.; Roger, T.; Faccio, Daniele Franco Angelo; Wright, E. M.

Link to publication in Heriot-Watt Research Gateway

Dichroism for orbital angular momentum using parametric amplification

J. Lowney,[1] T. Roger,[2] D. Faccio,[1,2] and E. M. Wright[1,*]

[1]*College of Optical Sciences, University of Arizona, Tucson, Arizona 85721-0094, USA*

[2]*Institute of Photonics and Quantum Sciences, School of Engineering and Physical Sciences, Heriot-Watt University,*
EH14 4AS Edinburgh, United Kingdom

We theoretically analyze parametric amplification as a means to produce dichroism based on the orbital angular momentum (OAM) of an incident signal field. The nonlinear interaction is shown to provide differential gain between signal states of differing OAM, the peak gain occurring at half the OAM of the pump field.

I. INTRODUCTION

One usage of the term dichroism in optics is to describe the differential loss of monochromatic light in one of two orthogonal polarization states with respect to some reference axis. This definition encompasses the case of both linear and circular dichroism and also gain and/or loss if one allows for negative absorption. For example, circular dichroism refers to the case in which right-handed circular (RHC) and left-handed circular (LHC) polarizations experience different propagation losses in the dichroic medium. As is well known, the RHC and LHC polarized states represent two orthogonal spin angular momentum (SAM) states for the light field. Then another way to express circular dichroism is that it is a dichroism based on the SAM state of the incident light field, or simply dichroism for SAM.

The goal of this paper is to propose and theoretically investigate parametric amplification as a means to produce dichroism based on the orbital angular momentum (OAM) of an incident signal field. The parametric interaction is shown to provide differential gain between signal states of differing OAM, the peak gain occurring at half the pump field OAM. Parametric interactions involving fundamental and second-harmonic fields carrying OAM have previously been explored both experimentally and theoretically, but mainly in the context of the conservation of OAM [1–3] as opposed to creating dichroism for OAM. A recent paper discussed circular dichroism that has its origin in the OAM of a beam incident on a nonchiral structure [4], whereas here we elucidate a means to produce dichroism that acts on the incident beam OAM directly.

The remainder of this paper is organized as follows. Section II describes the geometry and governing equations for our system and Sec. III presents a simplified analytic theory of parametric amplification and dichroism for OAM for pump and signal beams that are perfect optical vortices. In Sec. IV numerical results are presented for the case of signal and pump fields that are imperfect optical vortices and also signal fields that are Laguerre-Gaussian beams. Specifically, we demonstrate that parametric amplification can be used to create gain for a band of OAM states of an incident signal beam with absorption outside this band. A summary and conclusions are given in Sec. V.

---

*Corresponding author: ewan@optics.arizona.edu

II. BASIC GEOMETRY AND EQUATIONS

Our basic model involves propagation in the transparency region of a uniaxial nonlinear optical crystal. More specifically, we consider propagation along a principal axis to avoid the effects of beam walkoff and assume type-I phase-matching conditions. In our model of parametric amplification a signal field at the fundamental frequency ω_1 is incident on the crystal along with a pump field at the second-harmonic (SH) frequency $\omega_2 = 2\omega_1$. In this case the parametric interaction will generate an idler field at the fundamental frequency $\omega_3 = \omega_2 - \omega_1 = \omega_1$. For the type-I phase matching assumed, the signal field and idler fields are ordinary waves of refractive index n_1 and the pump is an extraordinary wave with refractive index n_2. Then, choosing the z axis as the propagation direction, denoting the complex slowly varying field amplitudes of the fundamental and SH fields as $A_1(x,y,z)$ and $A_2(x,y,z)$, and following the derivation and notation of Ref. [5], we obtain the paraxial wave equations for the fundamental ($j = 1$) and pump ($j = 2$) fields

$$
\begin{aligned}
\frac{\partial A_1}{\partial z} &= \frac{i}{2k_1}\nabla_\perp^2 A_1 + \frac{2i\omega_1^2 d_{\text{eff}}}{k_1 c^2} A_2 A_1^* e^{-i\Delta k z}, \\
\frac{\partial A_2}{\partial z} &= \frac{i}{2k_2}\nabla_\perp^2 A_2 + \frac{i\omega_2^2 d_{\text{eff}}}{k_2 c^2} A_1^2 e^{i\Delta k z},
\end{aligned}
\tag{1}
$$

where $\nabla_\perp^2 = \frac{\partial^2}{\partial x^2} + \frac{\partial^2}{\partial y^2}$ is the transverse Laplacian describing beam diffraction, d_{eff} is the effective nonlinear coefficient, $k_j = n_j\omega_j/c$ gives the z component of the wave vector for the two fields, and $\Delta k = 2k_1 - k_2$ is the wave-vector mismatch. We note that in this formulation the fundamental field incorporates both the signal and idler fields. Throughout this paper we assume the case of noncritical phase matching in a lithium triborate (LBO) crystal and a fundamental wavelength of $\lambda_1 = 1.064$ μm for which $n_1 = n_2 = n = 1.6$, $\Delta k = 0$, and $d_{\text{eff}} = 0.83$ pm/V. Then introducing the parameter $\eta = 2\omega_1 d_{\text{eff}}/n_1 c$, the propagation equations may be written as

$$
\begin{aligned}
\frac{\partial A_1}{\partial z} &= \frac{i}{2k_1}\nabla_\perp^2 A_1 + i\eta A_2 A_1^*, \\
\frac{\partial A_2}{\partial z} &= \frac{i}{4k_1}\nabla_\perp^2 A_2 + i\eta A_1^2.
\end{aligned}
\tag{2}
$$

These propagation equations for parametric amplification are to be solved for input fields that have cylindrically symmetric intensity profiles and carry OAM specified by the winding

numbers m_1 for the signal and m_2 for the pump

$$A_j(x,y,z=0) = \alpha_j U_j(\rho, z=0)e^{im_j\phi}, \quad j=1,2, \quad (3)$$

where (ρ, ϕ) are the transverse coordinates in cylindrical coordinates and the complex coefficients α_j are used to control the input powers of the fundamental and second-harmonic fields along with the relative phase θ between the input fundamental and SH fields. Here $U_j(x,y,z) \equiv U_j(\rho,z)$ are normalized cylindrically symmetric field profiles obeying

$$\int_{-\infty}^{\infty} dx \int_{-\infty}^{\infty} dy |U_j(x,y,z)|^2 = \int_0^{\infty} 2\pi\rho d\rho |U_j(\rho,z)|^2 = 1, \quad (4)$$

which describe the input fields at $z=0$ and their linear propagation to the output at $z=L$. The output powers in the fundamental and SH fields can be expressed as

$$P_j(L) = 2\epsilon_0 nc \int_{-\infty}^{\infty} dx \int_{-\infty}^{\infty} dy |A_j(x,y,L)|^2, \quad j=1,2, \quad (5)$$

and we note that $P_1(L)$ represents the total fundamental output power, signal plus idler. We furthermore define the output signal power

$$P_s(L)$$
$$= 2\epsilon_0 nc \left| \int_{-\infty}^{\infty} dx \int_{-\infty}^{\infty} dy U_1^*(x,y,L)e^{-im_1\phi} A_1(x,y,L) \right|^2, \quad (6)$$

which represents the power contained in the fundamental field projected onto the normalized input signal mode $U_1(x,y,L)e^{im_1\phi}$ evaluated at the output. In particular, $P_s(L)$ provides a measure of the output power associated with the input signal winding number m_1. In the following we shall examine the net gain for the fundamental field

$$G = \frac{P_1(L)}{P_{\text{sig}}}, \quad (7)$$

$P_{\text{sig}} = P_1(0)$ being the input signal power, and the signal gain

$$G_s = \frac{P_s(L)}{P_{\text{sig}}}. \quad (8)$$

In general, $P_1(z) > P_s(z)$ and $G > G_s$ since the nonlinear interaction will generate an idler field at the fundamental frequency from the pump and signal fields. We shall always choose the input pump power somewhat larger than the signal power to avoid excessive pump depletion.

III. SIMPLIFIED ANALYTIC THEORY

To set the stage for our numerical simulations we first present a simplified analytic theory of parametric amplification with OAM and associated dichroism. In particular, we consider the case that both the signal and pump beams are perfect optical vortices (POVs) [6,7]. A perfect optical vortex of winding number m has a narrow ring intensity profile with an azimuthal phase twist of $2\pi m$ in the transverse plane of the field. The key to using POVs is that the ring radius R should be independent of winding number and the same for all interacting fields. This choice maximizes the spatial overlap of the interacting fields and allows for a treatment that removes issues related

to the radial profile of the fields while retaining the azimuthal variation.

A. Perfect optical vortices

We first present a representation of a monochromatic POV with frequency $\omega = 2\pi c/\lambda$ and winding number m propagating in a medium of refractive index n. The POV has a ring-shaped intensity profile of radius R and width W, $R \gg W \gg \lambda$, along with a helical phase front of winding number m. (In the ideal case the ring width W would be zero [6].) We assume that the width W of the POV is sufficiently narrow compared to the ring radius that we may evaluate the properties of the beam around the peak of the ring. Then, for a POV with azimuthal variation $e^{im\phi}$ propagating along the z axis, the corresponding spiraling wave vector may be written as [8]

$$\vec{K} = K_x \vec{e}_x + K_y \vec{e}_y + K_z \vec{e}_z$$
$$= \frac{m}{R}\cos(\phi)\vec{e}_x + \frac{m}{R}\sin(\phi)\vec{e}_y + K_z\vec{e}_z, \quad (9)$$

with $R \gg \lambda$ the ring radius. By demanding that $K = k = 2\pi n/\lambda$ we obtain for a forward propagating field

$$K_z = \sqrt{k^2 - \frac{m^2}{R^2}} \approx k - \frac{1}{2k}\frac{m^2}{R^2}, \quad (10)$$

so we get the expected reduction in the z component of the wave vector due to the skewing associated with the helical phase front of the POV [9].

Based on the above results, the slowly varying electric field envelope for a POV evaluated around the peak of the ring may be written as

$$A(\rho = R, \phi, z) = a(z)e^{im\phi}e^{-(iz/2k)(m^2/R^2)}. \quad (11)$$

Then approximating the field of the POV as constant over its cross section, the power may be evaluated as

$$P(z) = 2\epsilon_0 nc 2\pi RW |a(z)|^2. \quad (12)$$

The utility of this solution rests on the Rayleigh range $z_R = kW^2/2$ being larger than the medium length L so that the ring width will vary little under propagation through the medium.

In the next subsection we consider a superposition of POVs at the fundamental frequency but with different winding numbers to capture both the signal and idler fields.

B. Parametric amplification

For this development we assume that the pump field ($j=2$) is much stronger than the signal field ($j=1$). Then the parametric amplification process, which produces one signal and one idler photon from one pump photon, generates an idler field ($j=3$) that has winding number $m_3 = m_2 - m_1$. Assuming that all fields are described by POVs, we then write the slowly varying electric fields for the fundamental and second harmonic fields, with $\rho = R$, as

$$A_1(\phi,z) = a_1(z)e^{im_1\phi}e^{-(iz/2k_1)(m_1^2/R^2)}$$
$$\qquad + a_3(z)e^{im_3\phi}e^{-(iz/2k_1)(m_3^2/R^2)},$$
$$A_2(\phi,z) = a_2 e^{im_2\phi}e^{-(iz/2k_2)(m_2^2/R^2)}, \quad (13)$$

with a_2 independent of z in the undepleted pump beam approximation and $a_3(0) = 0$ with no idler present at the input. Here we have set $k_3 = k_1$ since the signal and idler have the same frequency, and type-I phase matching is employed so the signal and idler experience the same refractive index. In the Appendix we show that using the fields in Eqs. (13) along with the propagation equations (2) yields the linearized signal-idler equations

$$\frac{da_1}{dz} = i(\eta a_2)a_3^* e^{i\kappa z}, \quad \frac{da_3}{dz} = i(\eta a_2)a_1^* e^{i\kappa z}, \quad (14)$$

where the OAM-dependent wave-vector mismatch for the process is

$$\kappa = \frac{(m_1 - m_2/2)^2}{k_1 R^2} \quad (15)$$

and we note that phase matching $\kappa = 0$ requires $m_1 = m_2/2$. These equations may be solved for the fields at the output of the crystal of length L [5],

$$a_1(L) = a_1(0)\left(\cosh(gL) - \frac{i\kappa}{2g}\sinh(gL)\right)e^{i\kappa L/2},$$

$$a_3(L) = a_1^*(0)\left(\frac{i\eta a_2}{g}\right)\sinh(gL)e^{i\kappa L/2}, \quad (16)$$

where $g = \sqrt{\eta^2|a_2|^2 - \kappa^2/4}$ is the growth rate if the argument of the square root is positive. The field intensities are given by $I_j(z) = 2\epsilon_0 nc|a_j(z)|^2$ in terms of which the growth rate may be written as

$$g = \sqrt{\beta I_p - \kappa^2/4}, \quad (17)$$

with $I_p = I_2(0)$ is the pump intensity at the peak of the ring and $\beta = 2\omega_1^2 d_{\text{eff}}^2/\epsilon_0 n^3 c^3$. Using Eq. (12), the input signal power is $P_{\text{sig}} = 2\epsilon_0 nc2\pi RW|a_1(0)|^2$, the output fundamental power is $P_1(L) = 2\epsilon_0 nc2\pi RW[|a_1(L)|^2 + |a_3(L)|^2]$, and the output signal power is $P_s(L) = 2\epsilon_0 nc2\pi RW|a_1(L)|^2$. Then the net gain for the fundamental field may be expressed as

$$G = \frac{P_1(L)}{P_{\text{sig}}} = \left|\cosh(gL) - \frac{i\kappa}{2g}\sinh(gL)\right|^2$$

$$+ \left|\frac{\eta a_2}{g}\sinh(gL)\right|^2 \quad (18)$$

and the signal gain becomes

$$G_s = \frac{P_s(L)}{P_{\text{sig}}} = \left|\cosh(gL) - \frac{i\kappa}{2g}\sinh(gL)\right|^2. \quad (19)$$

Note that under phase matching $\kappa = 0$ the peak signal gain is

$$G_{\text{peak}} = \cosh^2(\sqrt{\beta I_p}L), \quad (20)$$

which increases with pump intensity.

In summary, the simplified analytic solution demonstrates that phase matching for the parametric amplification process depends on the combination of the winding numbers of the signal and pump beams

$$\Delta = m_1 - \frac{m_2}{2}, \quad (21)$$

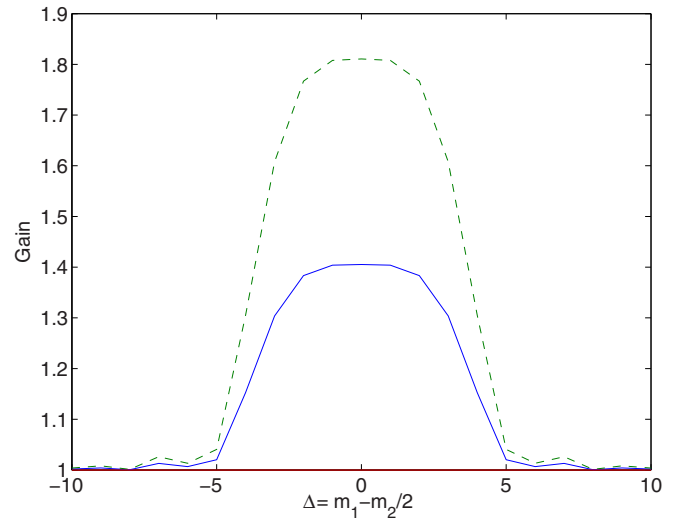whereas the peak signal gain varies with the input intensity.

FIG. 1. (Color online) Signal gain G_s (solid line) and net gain (dashed line) versus the OAM difference $m_1 - m_2/2$ for a LBO crystal of length $L = 2$ mm, pump intensity $I_2 = 2$ GW/cm^2, and ring radius $R = 35$ μm. The discrete data points are connected by a solid line as a visual aid.

C. Dichroism for OAM

Figure 1 shows an illustrative example of the signal gain G_s (solid line) and net gain G (dashed line) versus the OAM difference $\Delta = m_1 - m_2/2$ for a LBO crystal of length $L = 2$ mm, pump intensity $I_p = 2$ GW/cm^2, and a ring radius $R = 35$ μm. We have chosen the example of a LBO crystal as it allows for the assumed noncritical phase matching and has a damage threshold that exceeds the intensities used for pulses shorter than a nanosecond. Figure 1 reveals that significant gain occurs for a limited range of OAM values centered on $\Delta = 0$, that is, around $m_1 = m_2/2$. The fact that the peak of the net gain defined in Eq. (7), which includes both the signal and idler, exceeds the peak of the signal gain defined in Eq. (8) reflects the fact that a significant idler intensity is generated in this example, but we note that gain appears over a similar range in both cases. The full width for the parametric gain profile may be estimated by requiring $\kappa L = \pi$ at the edges for the phase mismatch to diminish the gain, which yields

$$\delta\Delta = 2\sqrt{\frac{\pi k_1 R^2}{L}}. \quad (22)$$

This full width scales as $\delta\Delta \propto R/\sqrt{\lambda_1 L}$, which is analogous to the spiral bandwidth used in spontaneous parametric down-conversion if we replace the Gaussian waist of the pump beam with the ring radius [10–12]. For this reason we refer to $\delta\Delta$ as the spiral bandwidth. For the chosen parameters this yields a spiral bandwidth of $\delta\Delta = 9$ in reasonable agreement with Fig. 1. Note also that the spiral bandwidth is independent of the winding numbers of the incident fields.

The parametric amplification therefore provides differential gain between different OAM states of the signal beam and in this sense acts as a dichroic element based on the signal OAM with the peak gain centered at $m_1 = m_2/2$ and spiral bandwidth given by Eq. (22). Furthermore, if we choose $|m_2| > \delta\Delta$, then for $m_2 > 0$ we can create the situation such

that only OAM states with $m_1 > 0$ experience significant gain and vice versa for $m_2 < 0$.

This concludes our discussion of the simplified analytic theory. Next we turn to numerical simulations using more realistic and practical beam profiles that will expose more general features of parametric amplification and associated dichroism for OAM.

IV. NUMERICAL SIMULATIONS

In this section we present numerical simulations of parametric amplification for more realistic types of input beams. The simulations are based on Eqs. (2) with initial conditions corresponding to signal and pump beams carrying OAM as in Eqs. (3). A standard beam propagation method is employed for the nonlinear propagation [13].

A. Imperfect optical vortices

Here we consider input beams that have a ring structure plus helical phase fronts, but they are not ideal POVs, so we term them imperfect optical vortices (IOVs). In particular, with reference to Eqs. (3), we write the radial profiles of the input fields as

$$U_j(\rho, z = 0) = \mathcal{N}_j \rho^{m_r} e^{-\rho^2/w_0^2}, \quad j = 1, 2, \quad (23)$$

where $\mathcal{N}_j$ are normalization constants, w_0 is a Gaussian beam waist, and m_r is a positive integer. Equations (23) describe annular beams of ring radius $R = w_0\sqrt{m_r/2}$ and for our numerics we choose $w_0 = 15 \ \mu\text{m}$, in which case the ring radius is $R = 35 \ \mu\text{m}$ for $m_r = 11$. We note that these initial conditions do not coincide with the familiar Laguerre-Gaussian modes of free space unless $|m_{1,2}| = m_r$, so these IOVs will generally change their functional form under linear propagation. For our parameters the fundamental Rayleigh range is $z_R \simeq 1$ mm, whereas the medium length is $L = 2$ mm, so the IOVs experience non-negligible diffraction over the medium length.

Figure 2 shows illustrative examples of parametric amplification using IOVs with parameters $m_r = 11$ and $w_0 = 15 \ \mu\text{m}$ giving $R = 35 \ \mu\text{m}$, an input pump power of $P_2(0) = 264$ kW, and a signal power of $P_{\text{sig}} = 0.2 P_2(0) = 52.8$ kW, these parameters yielding an intensity of $I_p = 8.8 \ \text{GW/cm}^2$ around the peak of the pump beam. The signal gain G_s given in Eq. (8) is plotted as a function of the OAM difference $\Delta = m_1 - m_2/2$ for the cases with $m_2 = 0$ (dotted line) and $m_2 = 11$ (solid line).

The results in Fig. 2(a) display qualitative similarities and differences with the simplified analytic theory in Fig. 1 that we now discuss. First, except for $\Delta = 0$, the results for the two different pump winding numbers $m_2 = 0, 11$ agree very well, this being expected from the simplified theory. However, for the case of zero winding number for both the pump and probe $m_1 = m_2 = \Delta = 0$ (dashed line), the signal gain shows an absorption dip. This arises since under this condition there is a resonant interaction between the injected fundamental field and the SH field that preserves the winding number of each field and depends on the relative phase θ between the signal and SH. For the case shown $\theta = \pi/4$ this yields absorption, whereas for $\theta = -\pi/4$ signal gain occurs [3]. In contrast, the
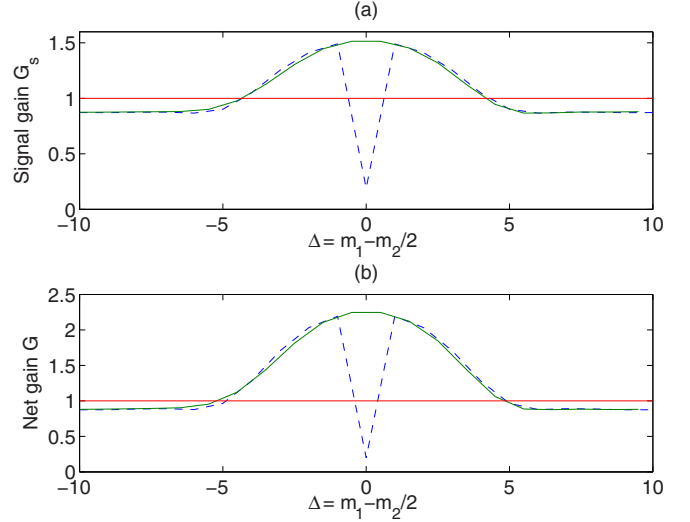

FIG. 2. (Color online) (a) Signal gain G_s versus the OAM difference $\Delta = m_1 - m_2/2$ for $m_2 = 0$ (dotted line) and $m_2 = 11$ (solid line) and (b) same as (a) but for the net gain G. The parameters used are for LBO and $m_r = 11$, $w_0 = 15 \ \mu\text{m}$, giving $R = 35 \ \mu\text{m}$, an input pump power of $P_2(0) = 264$ kW, and a signal power of $P_{\text{sig}} = 0.2 P_2(0) = 52.8$ kW, giving a peak intensity $I_p = 8.8 \ \text{GW/cm}^2$. The discrete data points are connected by a solid line as a visual aid.

case with $m_2 = 11$ shows no such absorption at $\Delta = 0$. This is because the resonant interaction between the fundamental and SH fields at $\Delta = 0$ requires $m_1 = m_2/2$, which cannot be satisfied for integer m_1 if m_2 is odd, but the absorption dip does appear at $\Delta = 0$ if m_2 is even. So excluding the dip at $\Delta = 0$, the results for $m_2 = 0, 11$ agree well. Note also that in Fig. 2(a) the signal gain turns to absorption for larger values of $|\Delta|$. This background absorption arises from conversion of the fundamental field with OAM m_1 to SH with OAM $2m_1$ (generally distinct from the input SH with OAM m_2.) The magnitude of this background absorption increases as the input signal power is increased. Furthermore, the width of the central peak in Fig. 2(a) is around 9, which is close to the spiral bandwidth $\delta\Delta = 9$ obtained from Eq. (22), the parameters being the same as in Fig. 1.

Figure 2(b) is the same as Fig. 2(a) but for the net gain given by the total fundamental output power divided by the input signal power. Figures 2(a) and 2(b) show the same features, but the net gains are larger than the signal gains due to the inclusion of the idler power in the net gain. The reason for this figure is to demonstrate that the common features appear in both gains and it is simpler to measure the net gain experimentally than to isolate the signal gain. Both gain measurements would demonstrate that the differential gain or loss between different signal OAM states depends on the OAM difference $\Delta = m_1 - m_2/2$.

Further features of the signal gain G_s are illustrated in Fig. 3. This figure shows the signal gain versus the OAM difference $\Delta = m_1 - m_2/2$ for the same parameters as in Fig. 2(a) with $m_2 = 11$ and pump intensities of $I_p = 8.8 \ \text{GW/cm}^2$ (solid line) and $I_p = 4.4 \ \text{GW/cm}^2$ (dashed line), the signal power being held constant at $P_{\text{sig}} = 52.8$ kW. As expected on the basis of Eq. (20), the peak signal gain increases with
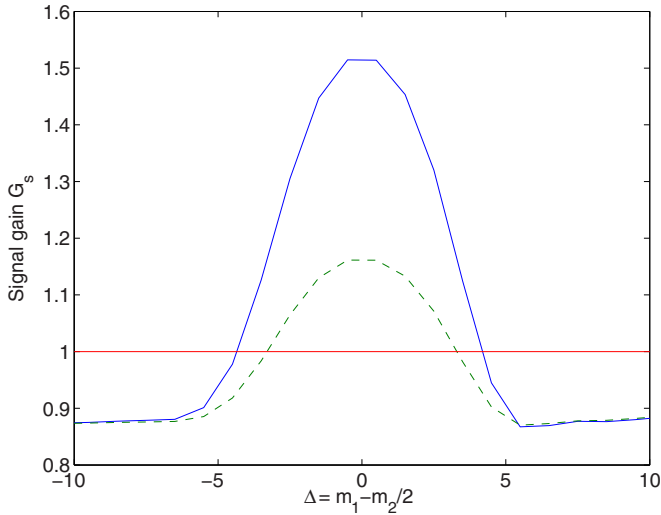
FIG. 3. (Color online) Signal gain G_s versus the OAM difference $\Delta = m_1 - m_2/2$ for the same parameters as in Fig. 2(a) with $m_2 = 11$ and a pump intensity of $I_p = 8.8$ GW/cm^2 (solid line) and $I_p = 4.4$ GW/cm^2 (dashed line), the signal power being held constant at $P_{\text{sig}} = 0.2P_2(0) = 52.8$ kW. The discrete data points are connected by a solid line as a visual aid.
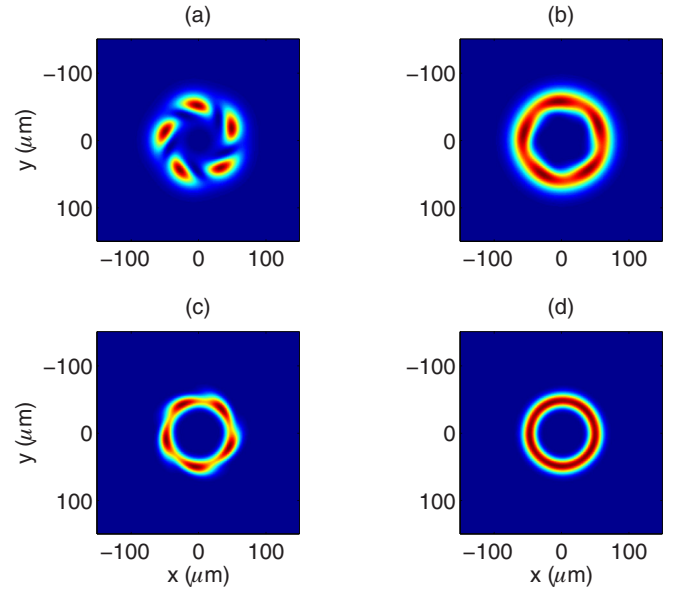

FIG. 4. (Color online) Examples of the (a) and (b) fundamental and (c) and (d) SH output transverse intensity profiles for two different values of the pump power: (a) and (c) $P_2(0) = 264$ kW and (b) and (d) $P_2(0) = 2.64$ kW, with $P_{\text{sig}} = 0.2P_2(0)$, all other parameters being the same as in Fig. 2. The winding numbers of the fundamental and SH fields were chosen as $m_1 = 8$ and $m_2 = 11$ so that $\Delta = 2.5$ and the generated idler will have winding number $m_3 = m_2 - m_1 = 5$.

pump intensity and given a peak signal gain of $G_{\text{peak}} = 1.5$ for the higher pump intensity, Eq. (20) predicts $G_{\text{peak}} = 1.23$ for the lower pump intensity, in reasonable agreement with the numerics [recall that the simple theory does not account for the background absorption due to second-harmonic generation (SHG) that is present in the numerics]. In contrast, we see that the background absorption is the same in both cases. This follows since the background absorption arises from SHG of the fundamental field of winding number m_1 to create a SH field with winding number $2m_1$, distinct from the pump SH field with winding number $m_2 = 11$, and this depends dominantly on the signal properties alone, not the pump properties.

Figure 4 shows illustrative examples of the fundamental (top row) and SH (bottom row) output transverse intensity profiles for two different values of the pump power $P_2(0) = 2.64$ and 264 kW, with $P_{\text{sig}} = 0.2P_2(0)$, all other parameters being the same as in Fig. 2. The winding numbers of the fundamental and SH fields were chosen as $m_1 = 8$ and $m_2 = 11$ so that $\Delta = 2.5$, and the generated idler will have winding number $m_3 = m_2 - m_1 = 3$. For Figs. 4(a) and 4(c) the pump power is $P_2(0) = 264$ kW and the fundamental intensity profile in Fig. 4(a) shows a five-lobe structure that arises from azimuthal beating between the signal and idler fields with azimuthal periodicity $2\pi/|m_1 - m_3| = 2\pi/5$. The pronounced lobes reflect the fact that a strong idler is generated in this case (as also evidenced by the difference between the net gain and signal gain in Fig. 2 for $\Delta = 2.5$). The five-lobe structure is also evident, but to a lesser degree, in the corresponding intensity profile for the SH shown in Fig. 4(c). Figures 4(b) and 4(d) show the same thing for a pump power $P_2(0) = 2.64$ kW, the key difference being that a weaker idler is generated and the five-lobe structure is less well pronounced. For even lower pump powers the intensity profiles tend closer

to rings. In summary, many of the features present in the simplified analytic model are also present using signal and pump beams that are IOVs. The simplified theory did not include the SHG process, so it did not account for the resonant SHG that occurs for $m_1 = m_2/2$ or the background absorption of the signal due to generation of a SH field at $m_2 = 2m_1$. The simplified model did capture the spiral bandwidth of the parametric amplification process. It then follows that the dichroism for OAM displayed by the simple model may also be realized using IOVs. A key distinction is that whereas the simplified analytic theory only shows differential gain between signal OAM states, the full theory with IOVs shows gain for a band of OAM states and loss outside that band and in this sense the full theory is richer.

B. Laguerre-Gaussian signal

For our second example we consider the case that the pump beam is an IOV as in Eq. (23) but the signal beam is a Laguerre-Gaussian (LG) beam. For input beams other than POVs or IOVs the spatial overlap of the signal and pump beams introduces features beyond the simplified theory and we use the LG beams as an illustrative example due to their relative ease of generation in the laboratory. In particular we consider LG signal modes with radial mode index $p = 0$ and winding number m_1,

$$U_1(\rho, z = 0) = \mathcal{N}_j \rho^{|m_1|} e^{-\rho^2/w_0^2}, \tag{24}$$

the pump IOV and signal LG beam being based on the same Gaussian spot size w_0. For $m_1 = 0$ this is a Gaussian beam peaked on axis, whereas for $m_1 \neq 0$ this is a ring beam with radius $R_1 = w_0\sqrt{|m_1|/2}$, so the ring radius varies with
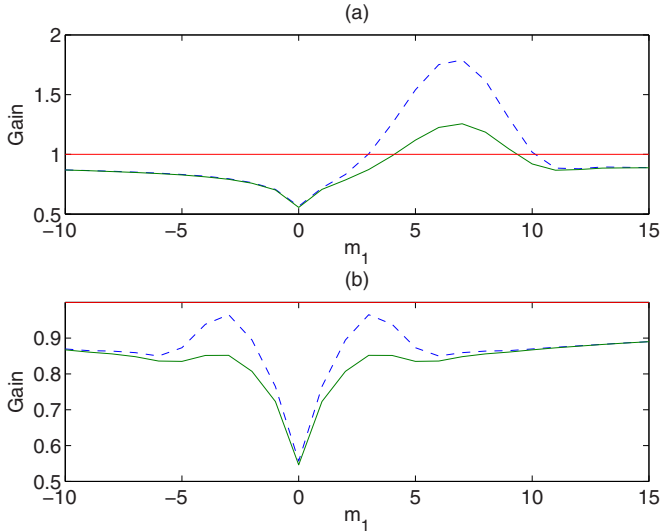
FIG. 5. (Color online) Plot of the signal gain G_s (solid line) and net gain G (dashed line) as functions of the signal beam winding number m_1 for a pump winding number (a) $m_2 = 11$ and (b) $m_2 = 0$. The parameter values are $m_r = 11$ and $w_0 = 15 \mu$m, giving $R = 35 \mu$m, an input pump power of $P_2(0) = 264$ kW, and a signal power of $P_{sig} = 0.2 P_2(0) = 52.8$ kW. The discrete data points are connected by a solid line as a visual aid.

winding number in contrast to the IOVs. For a pump beam that is an IOV as in Eq. (23) the ring sizes of the LG signal and pump beam will coincide when $m_r = |m_1|$.

Figure 5 shows illustrative examples of parametric amplification using LG signal beams with parameters $m_r = 11$ and $w_0 = 15 \mu$m giving $R = 35 \mu$m, an input pump power of $P_2(0) = 264$ kW, and a signal power of $P_{sig} = 0.2 P_2(0) = 52.8$ kW, these parameters yielding an intensity of $I_p = 8.8$ GW/cm^2 around the peak of the pump beam. In Fig. 5(a) the signal gain G_s (solid line) and net gain G (dashed line) are shown as a function of the signal beam winding number m_1 for a pump winding number $m_2 = 11$. This figure shows that parametric gain occurs over a band of winding numbers with peak gain centered around $m_1 \simeq 7$, with absorption outside of this gain band. The gain peak is shifted with respect to the phase-matching condition $m_1 = m_2/2 = 5.5$, but this is not surprising since the overlap between the interacting fields, which enters into the strength of the parametric wave interaction, varies with m_1. Although the gain profile is asymmetric, the results in Fig. 5(a) largely conform to the findings based on the using IOVs. This example demonstrates that by judicious choice of signal mode structure we can create the dichroism for OAM we elucidated using POVs.

The big difference for LG beams occurs when the winding number of the pump is changed and is illustrated for $m_2 = 0$ in Fig. 5(b), which shows the signal gain G_s (solid line) and net gain G (dashed line) as a function of the signal beam winding number m_1. In contrast to the case of IOVs where changing m_2 would simply shift the gain profile along the m_1 axis (see Fig. 2), the gain profiles in Fig. 5(b) are distinctly different from those in Fig. 5(a). In particular, for the chosen example the signal field experiences absorption for all values of m_1 (we chose the relative phase $\theta = \pi/4$

so that there is absorption at $m_1 = 0$). This arises since the phase-matching condition for peak gain now occurs at $m_1 = 0$, but there is little overlap between the signal and SH fields at that point and therefore little concomitant parametric gain to overcome losses due to second-harmonic generation. The main observation is that for more general signal and pump beam profiles the gain profile depends on the signal and probe winding numbers independently and not just through the OAM difference $\Delta = m_1 - m_2/2$.

V. SUMMARY AND CONCLUSIONS

In summary, we have investigated parametric amplification as a means to produce dichroism based on the orbital angular momentum of an incident signal field. Specifically, we have demonstrated that parametric amplification can be used to create gain for a band of OAM states of an incident signal beam with absorption outside this band. The spiral bandwidth of the gain was shown to depend on beam parameters and the medium length, whereas the peak gain occurs for a signal OAM equal to half that of the pump field and the peak signal gain increases with the pump power. This illustrates that parametric amplification can be used to provide significant gain to a particular sign of the probe OAM, which could in turn be used, for example, to sculpt the OAM content of an incident signal beam or bias the oscillating OAM states in an active system such as a laser. In a similar manner this dichroism could be used to vary the gain for a specific probe OAM dependent on the sign of the OAM of the pump and this could be used for all-optical switching of the probe.

To conclude, we remark that the results in Fig. 5 bear some resemblance to those predicted by Zel'dovich in the early 1970s [14]. More specifically, the Zel'dovich effect involves light scattering from an absorbing cylinder. If the cylinder is not rotating then a probe field incident radially onto it will suffer some absorption. Zel'dovich showed that if the cylinder is rotating then the probe can experience gain over a range of probe winding numbers, the required energy coming from the energy that needs to be added to sustain the rotation [14,15]. The Zel'dovich effect is therefore another system that can display dichroism for OAM. Another, closely related effect is Penrose superradiance, i.e., amplified scattering waves with angular momentum falling into a rotating black hole [16]. To elucidate the analogy for the parametric amplification system, the role of the cylinder is played by the second-harmonic pump and the role of the probe is played by the signal. In this analogy the probe experiences the refractive-index perturbation induced in the medium by the pump field via the second-order nonlinearity: This perturbation is rotating if $m_2 \neq 0$. More technically, parametric gain around the pump beam ring creates an ergoregion in which energy can be exchanged between fields of differing OAM as dictated by phase matching. Then the results in Fig. 5(b) show that if the cylinder (SH pump) is nonrotating, $m_2 = 0$, the probe is absorbed for all incident winding numbers, as expected for waves impinging on an absorbing, nonrotating cylinder or on a nonrotating black hole. In contrast, when the cylinder (pump beam) is rotating, gain becomes possible. Parametric amplification therefore provides a *nonlinear* analog system for the Zel'dovich effect. It is worth noting the similarities and

differences of the two systems: In the Zel'dovich effect, loss and gain are described by the same *linear* loss coefficient that changes sign depending only on the relative rotation frequencies of the cylinder and probe beam. In the nonlinear parametric amplification system, loss is represented by SHG that funnels energy from the probe into a SH signal that has different OAM with respect to the pump. Gain, on the other hand, is observed when the correct spatial phase relations are imposed between the pump and probe. Orbital angular momentum dichroism due to parametric amplification therefore depends on the phase properties of the probe (as in the Zel'dovich effect) and also of the pump. Notwithstanding this difference, the two processes are intriguingly similar, in that both display dichroism for OAM.

ACKNOWLEDGMENTS

APPENDIX: LINEARIZED SIGNAL-IDLER EQUATIONS

The utility of the POV solution introduced in Sec. III A rests on the Rayleigh range $z_R = kW^2/2$ being larger than the medium length L so that the ring width W will vary little under propagation through the medium. Within this approximation, the transverse Laplacian in cylindrical coordinates becomes $\nabla_\perp^2 \to \frac{1}{R^2}\frac{\partial^2}{\partial\phi^2}$, thereby neglecting radial expansion of the ring. Then treating the POV field in the vicinity of the ring

radius R as approximately constant over the cross section, $A_j(\rho = R, \phi, z) \approx A_j(\phi, z)$, the field equations (2) may be written along the top of the ring as

$$\frac{\partial A_1}{\partial z} - \frac{i}{2k_1 R^2}\frac{\partial^2 A_1}{\partial\phi^2} - i\eta A_2 A_1^* = 0, \qquad \text{(A1)}$$

$$\frac{\partial A_2}{\partial z} - \frac{i}{4k_1 R^2}\frac{\partial^2 A_2}{\partial\phi^2} = 0, \qquad \text{(A2)}$$

where we have used the undepleted pump beam approximation in Eq. (A2) and ignored the nonlinearity. Next the POV solutions in Eqs. (13) given by

$$A_1(\phi,z) = a_1(z)e^{im_1\phi}e^{-(iz/2k_1)(m_1^2/R^2)}$$
$$+ a_3(z)e^{im_3\phi}e^{-(iz/2k_1)(m_3^2/R^2)}, \qquad \text{(A3)}$$

$$A_2(\phi,z) = a_2 e^{im_2\phi}e^{-(iz/2k_2)(m_2^2/R^2)} \qquad \text{(A4)}$$

are used to express the propagating fields and note that, given $k_2 = 2k_1$, Eq. (A4) automatically satisfies (A2) with a_2 a constant. Substituting Eqs. (A3) and (A4) into Eq. (A1) and using $m_3 = m_2 - m_1$ yields

$$e^{im_1\phi}e^{-(iz/2k_1)(m_1^2/R^2)}[da_1/dz - i(\eta a_2)a_3^* e^{i\kappa z}]$$
$$+ e^{im_3\phi}e^{-(iz/2k_1)(m_3^2/R^2)}\left[\frac{da_3}{dz} - i(\eta a_2)a_1^* e^{i\kappa z}\right] = 0, \quad \text{(A5)}$$

with κ given by Eq. (15). Then setting terms with the same exponential azimuthal variation individually to zero, assuming $m_1 \neq m_3$, yields the linearized signal-idler equations (14).

[1] D. P. Caetano, M. P. Almeida, P. H. Souto Ribeiro, J. A. O. Huguenin, B. Coutinho dos Santos, and A. Z. Khoury, Phys. Rev. A **66**, 041801(R) (2002).

[2] J. A. O. Huguenin *et al.*, J. Mod. Opt. **53**, 647 (2006).

[3] F. Devaux and R. Passier, Eur. Phys. J. D **42**, 133 (2007).

[4] X. Zambrana-Puyalto, X. Vidal, and G. Molina-Terriza, Nat. Commun. **5**, 4922 (2014).

[5] R. W. Boyd, *Nonlinear Optics*, 3rd ed. (Academic, New York, 2008), Chap. 2.

[6] A. S. Ostrovsky, C. Rickenstorff-Parrao, and V. Arrizon, Opt. Lett. **38**, 534 (2013).

[7] M. Chen *et al.*, Opt. Lett. **38**, 4919 (2013).

[8] T. Roger, J. F. Heitz, E. M. Wright, and D. Faccio, Sci. Rep. **3**, 3491 (2013).

[9] K. Dholakia, N. B. Simpson, M. J. Padgett, and L. Allen, Phys. Rev. A **54**, R3742 (1996).

[10] F. M. Miatto, A. M. Yao, and S. M. Barnett, Phys. Rev. A **83**, 033816(R) (2011).

[11] M. McLaren, J. Romero, M. J. Padgett, F. S. Roux, and A. Forbes, Phys. Rev. A **88**, 033818 (2013).

[12] R. Ramírez-Alarcón, H. Crus-Ramírez, and A. B. U'Ren, Laser Phys. **23**, 055204 (2013).

[13] M. D. Fleck and J. A. Fleck, Appl. Opt. **19**, 1154 (1980).

[14] Y. B. Zel'dovich, Pis'ma Zh. Eksp. Teor. Fiz. **14**, 270 (1971) [JETP Lett. **14**, 180 (1971)]; Zh. Eksp. Teor. Fiz. **62**, 2076 (1972) [Sov. Phys. JETP **35**, 1085 (1972)].

[15] Ya. B. Zel'dovich, L. V. Rozhanskii, and A. A. Starobinskii, Izv. Vyssh. Uchebn. Zaved. Radiofiz. **29**, I008 (1986).

[16] R. Penrose, Gen. Relativ. Gravit. **34**, 1141 (2002) [reprinted from Riv. Nuovo Cimento Num. Spez. I, 257 (1969)].